

# Adiabatic, Shock, and Plastic Work Heating of Solids and Exploding Metal Cylinders

Edward L. Ruden, *Member, IEEE* and Gerald F. Kiuttu, *Member, IEEE*

**Abstract**—Solids subjected to high pressures, shocks, and/or deformation experience an increase in internal energy density and temperature due to adiabatic compression, shock heating, and plastic work heating, respectively. Analytic approximations are derived here for the internal energy and temperature changes that result from these processes based on the analytic constitutive model and Grüneisen equation of state of Steinberg. Although of general use, the utility of the expressions is demonstrated by the detailed example of a cylindrical metal tube filled with high explosives, and detonated on axis at one end. This geometry is often used to determine the detonation properties of high explosives, where it is known as the “cylinder test.” The geometry is also of special interest for use as the armature of cylindrical magnetic flux compression pulsed current generators. The results are favorably compared with two dimension numerical simulations of the process using Lawrence Livermore National Laboratory’s shock-hydro computer code CALE using the same model for the metal.

**Index Terms**—Cylinder test, detonation, Hugoniot, plastic flow, plasticity, shock heating, shock wave.

## I. INTRODUCTION

THIS paper was motivated by a need to better understand the thermodynamic evolution of explosively expanded metal tubes. AFRL’s Directed Energy Directorate (DE) is developing explosive axial magnetic flux compression (pulsed current) generators [1] (FCGs) suitable as the primary energy source for expendable devices requiring very high electrical pulsed power. These generators use a cylindrical metal armature filled with high explosive and detonated on axis at one end. This geometry is independently known as the “cylinder test” in explosives research, being well suited for the analysis of the properties of explosive products [2]. In the generator application, axial magnetic flux trapped between the expanding armature and a surrounding helically wound stator is compressed, generating high current. The shock to, and plastic expansion of the armature results in an increase in the armature’s temperature, leading to increased electrical resistivity and possible melting. If melting occurs, further flux compression is impaired by a greatly enhanced Rayleigh–Taylor instability. Even before melting, the expansion process itself can become unstable, with the armature fragmenting by plastic instability. These processes result in decreased performance, and more detailed modeling of them is necessary. The principal tool used

for modeling the pulsed power circuit is CAGEN [3], which couples a lumped circuit to a zero dimensional simulation of the generator for which the armature is characterized by its outer radius as a function of axial position and time  $R(z, t)$ . One application of results presented here is to improve the electrical resistivity treatment of the armature model in programs like CAGEN. Given additional simplifying assumptions, energy and temperature estimates are rendered in purely analytic form. In the process, analytic solutions to energy and temperature changes due to basic mechanical processes are derived based on Steinberg’s form [4] of the Grüneisen equation of state [5] and the Steinberg–Cochran–Guinan constitutive relations for material strength [6], hereafter referred to as the “Steinberg model.” These general solutions are the primary emphasis of this paper because of their wider potential interest, with the cylinder test application presented thereafter as a detailed example their utility.

The Steinberg model is a popular dynamic model of solids, especially metals, which undergo high rates of strain and compression ( $\gtrsim 10^5 \text{ s}^{-1}$ ). This model has been generalized for lower strain rates, where strain rate dependences are often significant [7]. The original strain rate independent model and, therefore, high strain rates will be assumed here, though. Many materials have been characterized for it [4], and it is used in several hydrodynamic and magnetohydrodynamic computer codes [8]–[13]. Despite the model’s analytic form, though, its potential for deriving approximate analytic solutions has not been well exploited. The more general expressions presented should prove to be useful tools for studying a wide variety of dynamically deforming geometries. The symbolic form of the expressions should make various dependences on variables more apparent and parameter space surveys easier to accomplish than with codes alone. Follow-up with computer modeling of promising configurations thereby identified may then be pursued more productively.

Section II reviews adiabatic compression in the Steinberg model and provides useful approximations for internal energy per unit mass  $E$  and temperature  $T$  along the adiabat. These expressions are needed to calculate  $T$  as a function of compression and  $E$  more generally. Section III derives  $E$  and  $T$  approximations that result from planar shocks traversing a solid with standard initial conditions. Section IV derives an expression for the change in  $E$  as a function of the equivalent deviatoric strain  $\epsilon$  resulting from plastic deformation. This expression is particularly useful because it takes into account the important effects of work hardening and thermal softening in the Steinberg model, although elasticity, compressibility, and

Manuscript received August 8, 2001; revised April 19, 2002.

The authors are with the Air Force Research Laboratory, Directed Energy Directorate, Kirtland AFB, NM 87117 USA.

Digital Object Identifier 10.1109/TPS.2002.805415

the pressure dependence of the yield strength are neglected. Section V presents a detailed example of how the derived expressions may be used for explosively expanded cylinders. Section VI presents results of two dimensional numerical simulations of this cylinder test for comparison with the analytic expressions to gauge how well the analytic approximations represent the Steinberg model. Discussion of the empirical validity of the model itself is covered in the supplied references and is considered beyond the scope of this paper.

One shortcoming of the approximations presented for shock heating and plastic work is that they assume both processes do not occur simultaneously. A more unified thermomechanical treatment is required, in particular, where shocks are strongly nonplanar, such as in impact cratering. Fortunately, there are many other cases where one process dominates the other or they occur on different time scales. The cylinder test presented is an example of the latter. Thermal conductivity is neglected throughout due to the short time scales of the processes involved.

## II. TEMPERATURE AND ADIABATIC HEATING

The Steinberg model's relationship between pressure  $P$ , density  $\rho$ , and internal energy per unit mass relative to that at standard conditions ( $P = 0$ , temperature  $T = T_R = 300$  K)  $E$  is [6]

$$P(\mu, E) = \begin{cases} \frac{\rho_0 C_0^2 \mu \left[ 1 + \left( 1 - \frac{\gamma_0}{2} \right) \mu - \frac{b}{2} \mu^2 \right]}{\left[ 1 - (S_1 - 1) \mu - S_2 \frac{\mu^2}{\mu+1} - S_3 \frac{\mu^3}{(\mu+1)^2} \right]^2} \\ \quad + (\gamma_0 + b\mu) \rho_0 E, & \text{if } \mu > 0 \\ \rho_0 C_0^2 \mu + \rho_0 \gamma_0 E, & \text{if } \mu \leq 0. \end{cases} \quad (1)$$

Here,  $\mu = \rho/\rho_0 - 1$  and  $C_0$  (sound speed),  $\rho_0$  (standard density),  $\gamma_0$ ,  $b$ ,  $S_1$ ,  $S_2$ , and  $S_3$  are available phenomenological parameters [4] described more fully in the references.

To find an expression for  $T$ , we start with  $T = (E - E_c)/C$  for fixed  $\mu$ , where  $C$  is the specific heat at constant volume (assumed constant in the Steinberg model) and  $E_c = E$  at compression  $\mu$  and  $T = 0$  [6]. Subtracting both sides of this equation, solved for the special case of the adiabat from standard conditions were  $T = T_0(\mu)$  and  $E = E_0(\mu)$ , from the respective sides of the general case results in

$$T(E, \mu) = T_0(\mu) + \frac{E - E_0(\mu)}{C}. \quad (2)$$

$T_0(\mu)$  may be found from the adiabatic relationship [14]

$$T_0 = T_R \exp \left[ - \int_{V_0}^V \frac{\gamma(V')}{V'} dV' \right] \quad \gamma(V) = V \left( \frac{\partial P}{\partial \mathcal{E}} \right)_V \quad (3)$$

where  $V$  is a sample volume (with  $V_0$  its standard conditions value),  $\mathcal{E}$  is internal energy, and  $\gamma$  is the Grüneisen ratio [14],

[4]. Changing variables via  $V = V_0/(\mu + 1)$  and  $\mathcal{E} = \rho_0 V_0 E$ , using (1) for  $P$ , and integrating

$$T_0(\mu) = \begin{cases} T_R (\mu + 1)^b \exp \left( \frac{(\gamma_0 - b)\mu}{\mu + 1} \right) & \text{if } \mu > 0 \\ T_R \exp \left( \frac{\gamma_0 \mu}{\mu + 1} \right) & \text{if } \mu \leq 0 \end{cases} \quad (4)$$

$$\gamma(\mu) = \frac{\gamma_0 + b\mu}{\mu + 1}.$$

This expression may be recognized as a generalization the Steinberg model's melting temperature [4], which is assumed to follow the adiabat.

$E_0(\mu)$ , meanwhile, may be found from Eq. (1) since  $d\mathcal{E} = -P dV$  along an adiabat. This results in the following differential equation and its solution [15],

$$\frac{dE}{d\mu} = \frac{P(\mu, E)}{\rho_0(\mu + 1)^2} \quad (5)$$

$$E_0(\mu) = \frac{T_0(\mu)}{\rho_0} \int_0^\mu \frac{P(\mu', 0)}{(\mu' + 1)^2 T_0(\mu')} d\mu'. \quad (6)$$

This expression may be approximated to within 2% in the specified ranges by

$$E_0(\mu) \approx \begin{cases} \frac{C_0^2 T_0(\mu)}{T_R} \sum_{i=2}^4 a_i \mu^i, & \text{if } 0 < \mu < 0.35 \\ \frac{C_0^2 T_0(\mu)}{T_R} \sum_{i=2}^5 b_i \mu^i, & \text{if } -0.20 < \mu \leq 0 \end{cases}$$

$$a_2 = \frac{1}{2} \quad a_3 = \frac{1}{6} (4S_1 - 6 - 3\gamma_0)$$

$$a_4 = 800 \exp \left( \frac{(b - \gamma_0)}{5} \right) \left( \frac{4}{5} \right)^b$$

$$\times \frac{40 - 4\gamma_0 - b}{(25S_1 + 5S_2 + S_3 - 125)^2}$$

$$- (2S_1 - 3 - \frac{3}{2}\gamma_0) - 4$$

$$b_2 = \frac{1}{2}; \quad b_3 = -\frac{1}{3} (2 + \gamma_0); \quad b_4 = \frac{1}{8} (6 + 6\gamma_0 + \gamma_0^2)$$

$$b_5 = \frac{4}{245} \left( -8192 \exp \left( \frac{\gamma_0}{7} \right) + 8134 + 1078\gamma_0 + 49\gamma_0^2 \right). \quad (7)$$

The coefficients are determined by Taylor expansion of the integrand of (6), except for  $a_4$  and  $b_5$ . For greater accuracy, the latter are chosen to make the integrand error zero at  $\mu' = -(1/8)$  and  $1/4$ .

## III. SHOCK HEATING

If we assume the external pressure rises instantaneously from 0 to a constant  $P_1$  upon the arrival of a planar shock wave through an initially stationary solid with standard conditions,

the shocked material properties can be described by the Hugoniot relations [16], expressible as

$$v_s^2 = \frac{(\mu_1 + 1)P_1}{\mu_1 \rho_0} \quad \mu_1 = \frac{\rho_1}{\rho_0} - 1$$

$$K_1 \equiv \frac{v_1^2}{2} = E_1 = \frac{\mu_1 P_1}{2\rho_0(\mu_1 + 1)}. \quad (8)$$

$\rho_1$ ,  $v_1$ ,  $P_1$ ,  $E_1$ , and  $K_1$  are density, velocity,  $P$ ,  $E$ , and kinetic energy per unit mass behind the shock, respectively, and  $v_s$  is shock speed. Substituting  $E_1$  in (8) into (1), with  $P = P_1$ , and solving for  $P_1$  gives us our Hugoniot function

$$P_1 = \frac{\rho_0 C_0^2 \mu_1 (\mu_1 + 1)}{\left[1 - (S_1 - 1)\mu_1 - S_2 \frac{\mu_1^2}{\mu_1 + 1} - S_3 \frac{\mu_1^3}{(\mu_1 + 1)^2}\right]^2}. \quad (9)$$

For modest compressions, we may neglect the  $S_2$  and  $S_3$  terms [17]. Equation (9), then, reduces to a quadratic in  $\mu_1$  with (meaningful) solution

$$\mu_1 = \frac{\sqrt{4\Pi S_1 + 1} - 2\Pi(S_1 - 1) - 1}{2 - 2\Pi(S_1 - 1)^2}, \quad \Pi = \frac{P_1}{\rho_0 C_0^2}. \quad (10)$$

Plugging this into [(8)] gives

$$v_s^2 = \frac{\Pi C_0^2}{\alpha_1} \quad K_1 \equiv \frac{v_1^2}{2} = E_1 = \frac{\alpha_1 \Pi C_0^2}{2} \quad (11)$$

$$\alpha_1 = \frac{\mu_1}{\mu_1 + 1} = \frac{\sqrt{4\Pi S_1 + 1} - 2\Pi(S_1 - 1) - 1}{\sqrt{4\Pi S_1 + 1} - 2\Pi S_1 (S_1 - 1) + 1}. \quad (12)$$

The temperature behind the shock is, from (2)

$$T_1 = T(E_1, \mu_1). \quad (13)$$

One important application to the solutions above is the case of an explosive detonation wave which interacts with a plate or shell. In this case, the initial shock compression unloads at the surface opposite the explosive, sending a continuous adiabatic rarefaction wave inward. Some energy is transmitted back into the explosive products, and some reflects as a second outward shock.  $E_1 - E_0(\mu_1)$  is the irreversible contribution to the energy behind the initial shock and is, therefore, a *lower bound* on the final energy  $E_s$  after the explosive products and waves dissipate, and pressure falls off. Before this, though, secondary shocks and rarefactions continue to increase heat and smooth the pressure profile, respectively. An *upper bound* on  $E_s$  is  $E_1$  itself, so we have

$$E_1 - E_0(\mu_1) \leq E_s \leq E_1. \quad (14)$$

To find the temperature corresponding to  $E = E_s$  after pressure fall off, we solve (1) for  $\mu = -\gamma_0 E/C_0^2$  (negative due to thermal expansion) at  $P = 0$  and plug into (2)

$$T = T(E, -\gamma_0 E/C_0^2) \quad (P = 0). \quad (15)$$

#### IV. PLASTIC WORK HEATING

The contribution to  $E$  from plastic work heating  $E_p$  as a function of  $E$ 's initial value  $E_s$  and equivalent plastic strain  $\epsilon$  may be derived in closed form for the Steinberg model, provided we neglect compressibility, elasticity, the pressure dependence of the uniaxial yield strength  $Y$ , and other active heat sources. The (usually more important) effects of work hardening and thermal softening of the material are retained, however. Though  $E_s$  is of arbitrary value in this section, we use the same symbol that was used for shock heating in the previous section to suggest one potential origin.

Neglecting elasticity, the Levy–Mises (L–M) relation for rigid plastic flow is [18]

$$\mathbf{D} \equiv \frac{1}{2}(\nabla \mathbf{v} + \nabla \mathbf{v}^T) = \frac{3}{2} \frac{d\epsilon}{dt} \frac{\mathbf{S}}{Y} \quad \epsilon \equiv \frac{2}{\sqrt{6}} \int \sqrt{\mathbf{D} \cdot \mathbf{D}} dt \quad (16)$$

where  $\mathbf{D}$  and  $\mathbf{S}$  are the deviatoric strain rate and stress tensors, respectively. The Steinberg model's strain rate independent material strength equation [6] is

$$Y = \left[1 + \frac{AP}{(1 + \mu)^{1/3}} - B(T - T_R)\right] \times \begin{cases} Y_0 [1 + \beta(\epsilon + \epsilon_i)]^n, & \text{if } \epsilon < \epsilon_c \\ Y_{\max}, & \text{if } \epsilon \geq \epsilon_c \end{cases} \quad (17)$$

where  $A$ ,  $B$ ,  $\beta$ ,  $n$ ,  $Y_{\max}$ , and  $Y_0$ , and  $\epsilon_i$  are phenomenological parameters tabulated for several materials [4], and

$$\epsilon_c = \frac{(Y_{\max}/Y_0)^{1/n} - 1}{\beta} - \epsilon_i. \quad (18)$$

We neglect the  $P$  dependent term in (17) and use, assuming incompressibility,  $(T - T_R) = E/C$ , from (2). Given these assumptions, the plastic work rate [18] per unit mass is, using (16) and (17)

$$\frac{dE_p}{dt} \equiv \frac{\mathbf{S} \cdot \mathbf{D}}{\rho} = \frac{Y}{\rho_0} \frac{d\epsilon}{dt} = \frac{1 - \frac{B}{C} E}{\rho_0} \frac{d\epsilon}{dt} \times \begin{cases} Y_0 [1 + \beta(\epsilon + \epsilon_i)]^n \\ Y_{\max} \end{cases} \quad (19)$$

where  $\rho_0$  is the standard mass density of the material (assumed constant). Here and henceforth, the upper and lower expressions are for  $\epsilon < \epsilon_c$  and  $\epsilon \geq \epsilon_c$ , respectively, unless otherwise specified. Assuming further that there is no other active heat source, then  $E = E_p + E_s$ , and (19) is reducible to a differential equation in  $E_p$  with reference to  $\epsilon$  with solution

$$E_p = \left(\frac{C}{B} - E_s\right) - \left(\frac{C}{B} - E_s\right) \times \begin{cases} \exp\left[-\frac{BY_0}{C\rho_0\beta(n+1)} \left([1 + \beta(\epsilon + \epsilon_i)]^{n+1} - [1 + \beta\epsilon_i]^{n+1}\right)\right] \\ \exp\left[-\frac{BY_0}{C\rho_0\beta(n+1)} \left([1 + \beta(\epsilon_c + \epsilon_i)]^{n+1} - [1 + \beta\epsilon_i]^{n+1}\right) - \frac{BY_{\max}}{C\rho_0} (\epsilon - \epsilon_c)\right] \end{cases} \quad (20)$$

Note, if thermal softening is neglected, one must take the limit of  $B \rightarrow 0$ , or (better yet) resolve (19) with  $B = 0$ ,

$$\lim_{B \rightarrow 0} E_p = \begin{cases} \frac{Y_0}{\rho_0 \beta (n+1)} \left( [1 + \beta(\epsilon + \epsilon_i)]^{n+1} - [1 + \beta\epsilon_i]^{n+1} \right) \\ \frac{Y_0}{\rho_0 \beta (n+1)} \left( [1 + \beta(\epsilon_c + \epsilon_i)]^{n+1} - [1 + \beta\epsilon_i]^{n+1} \right) \\ + \frac{Y_{\max}}{\rho_0} (\epsilon - \epsilon_c). \end{cases} \quad (21)$$

$E = E_s + E_p$  may now be used in (15) to determine the temperature.

## V. EXAMPLE—EXPLOSIVELY EXPANDED TUBE

### A. Geometry

We consider the example of a long (compared to its diameter) cylindrical tube of ductile metal loaded with high explosive and detonated on axis at one end. Upper and lower bounds on the shock heating of the tube, an estimate of the subsequent plastic work heating as the tube wall flares outward into a cone, and (as a caveat) the critical radius for the onset of plastic instability are derived. Much analytic theory [19]–[22], computational modeling [23], [2], and experimental results [20], [24], [2] have been published on the this geometry, with details of the detonation wave and explosive products properties and interaction particularly well covered. Emphasis here will be placed instead on the thermal response of the tube material itself. Fortunately, for the simplest approximations presented, effects of the explosive products on shock heating and plastic work as a function of the expanding radius of the cylinder can be parameterized by the pressure  $P_1$  behind the initial shock that traverses the tube wall after the detonation wave passes and the ratio  $V_r/D$ , where  $V_r$  is the radial expansion speed of the tube after it has expanded by a significant amount relative to the initial radius and  $D$  is the detonation speed. Existing models to estimate these two parameters are referenced.

### B. Initial Shock Heating

The detonation wave in the subject case is primarily transverse to the inner cylinder wall.  $P_1$  may be estimated by an available model [25] which assumes the explosive products can be described by Prandtl–Meyer flow around a sharp corner [26] with a self-consistently determined angle created by the compression of the tube wall due to the first shock. A necessary condition for this is that  $D$  be larger than the shock speed in the solid. This is the case for most high explosives on metals other than Be. An ideal gas with constant gamma adiabatic law for the products with the Chapman–Jouget (C–J) values for the

initial pressure  $P_j$ , density  $\rho_j$ , and particle speed  $v_j$  behind the shock are assumed [27], [28]

$$\begin{aligned} P &= P_i \left( \frac{\rho}{\rho_j} \right)^{\gamma_j} & P_j &= \frac{\rho_x D^2}{\gamma_j + 1} \\ \rho_j &= \frac{\gamma_j + 1}{\gamma_j} \rho_x & v_j &= \frac{D}{\gamma_j + 1}. \end{aligned} \quad (22)$$

Here,  $\rho_x$  is the explosive's initial density, and  $\gamma_j$  is a phenomenological parameter. Higher order shock terms  $S_2$  and  $S_3$  in the metal's EOS are neglected, as was done in Section III.

To simplify Neal's solution to  $P_1$ , we note the integral required to obtain the plate surface deflection angle  $\alpha$ , based on the explosive product response [Neal's (6)], has the solution

$$\begin{aligned} \alpha &= \sqrt{\frac{\gamma_j + 1}{\gamma_j - 1}} \arccos \eta - \frac{1}{2} \left( \arccos \frac{\sqrt{\gamma_j + 1} \eta + \sqrt{2}}{\sqrt{\gamma_j + 1} + \sqrt{2} \eta} \right. \\ &\quad \left. + \arccos \frac{\sqrt{\gamma_j + 1} \eta - \sqrt{2}}{\sqrt{\gamma_j + 1} - \sqrt{2} \eta} \right) \end{aligned} \quad (23)$$

where  $\eta$  is defined in (24).  $\eta$  may also be expressed in terms of the angle  $\theta$  between the metal shock front and the  $z$ -axis with the help of the equations which describe the metal's selfconsistent response to  $P_1$  [Neal's (10) and (12)]

$$\begin{aligned} \eta &\equiv \left( \frac{P_1}{P_j} \right)^{(\gamma_j - 1)/2\gamma_j} \\ &= \left( \frac{\rho_0 D^2}{P_j} \left( 1 - \frac{D(S_1 - 1) \sin \theta + C_0}{D S_1 \sin \theta} \right) \sin^2 \theta \right)^{(\gamma_j - 1)/2\gamma_j}. \end{aligned} \quad (24)$$

Meanwhile, Neal's (12) solved for  $\alpha$  is

$$\alpha = \theta - \arctan \left( \frac{D(S_1 - 1) \sin \theta + C_0}{D S_1 \cos \theta} \right). \quad (25)$$

Intersecting this with (23), using the second expression in (24) for  $\eta$ , gives  $\theta$  and therefore, from (24),  $P_1$ . A good starting point for Newton's method to find this intersection is the average of

$$\theta_{\min} = \arcsin \left( \frac{C_0}{D} \right)$$

and

$$\theta_{\max} = \arcsin \frac{\rho_0 C_0 + \sqrt{\rho_0^2 C_0^2 + 4 \rho_0 P_j S_1}}{2 \rho_0 D}. \quad (26)$$

$\theta_{\min}$  corresponds to the acoustic limit for metal shock speed, and  $\theta_{\max}$  corresponds to  $\eta = 1$  ( $P_1 = P_j$ ) in (24). There is no real and meaningful solution to (23) outside this range. Generally speaking, one obtains values of  $P_1$  for the metal shock roughly half that obtained from the more commonly treated case of the interaction of a detonation wave normally incident to the interface [29].

After obtaining an estimate of  $P_1$ ,  $E_1$  and bounds on  $E_s$  may be found from (11) and (14), respectively.

### C. Subsequent Plastic Deformation

Given an axisymmetric thin-walled shell of radius  $R = R(z, t)$  expanding at radial velocity  $V = V(z, t)$ , and zero axial velocity, nonzero components of  $\mathbf{D}$  and  $\epsilon$  are, from (16)

$$(D_{rr}, D_{\theta\theta}, D_{zz}) = (-1, 1, 0) \frac{V}{R} \quad D_{rz} = D_{zr} = \frac{1}{2} \frac{\partial V}{\partial z} \quad (27)$$

$$\epsilon = \frac{2}{\sqrt{3}} \int \left[ \left( \frac{V}{R} \right)^2 + \left( \frac{1}{2} \frac{\partial V}{\partial z} \right)^2 \right]^{1/2} dt. \quad (28)$$

In a thin shell model where  $R(z, t)$  is independently determined and there are no other active heat sources, (28) may be plugged into (20) directly to determine  $E_p(z, t)$ . On the other hand, if other active sources of heat are present, differentiating (28) w.r.t.  $t$  and plugging into (19) gives us the more general expression for the plastic work contribution to the heating rate

$$\frac{dE_p}{dt} = \frac{2(1 - \frac{B}{C}E)}{\sqrt{3}\rho_0} \left[ \left( \frac{V}{R} \right)^2 + \left( \frac{1}{2} \frac{\partial V}{\partial z} \right)^2 \right]^{1/2} \times \begin{cases} Y_0 [1 + \beta(\epsilon + \epsilon_i)]^n \\ Y_{\max}. \end{cases} \quad (29)$$

To simplify things further, a reasonable estimate of the plastic heating may be made by using the following approximations for  $V$  and, from (28),  $\epsilon$

$$V = V_r \Theta(Dt - z) \quad (30)$$

$$\epsilon = \frac{2}{\sqrt{3}} \ln \frac{R}{R_0} + \frac{V_r}{\sqrt{3}D}, \quad \text{for } t > \frac{z}{D}. \quad (31)$$

Here,  $V_r$  and  $D$  are the radial expansion velocity and the axial explosive detonation velocity, respectively, and both are assumed constant.  $\Theta(z)$  is the Step Function. In other words, we assume the armature is stationary until a purely axial shock front passes, at which time the armature is instantaneously accelerated to radial velocity  $V_r$ , flaring out into a conical shape. The simplest approximation for  $V_r$ , meanwhile, is provided by the Gurney Equation [19], [22]

$$V_r = \sqrt{2E_x} \left( \frac{M}{M_x} + \frac{1}{2} \right)^{-1/2} \quad (32)$$

where  $M$  is the total cylinder mass, and  $M_x$  and  $E_x$  are the total explosive mass and phenomenological ‘‘Gurney energy’’ (liberated chemical energy per unit mass), respectively. Given  $V_r$  and  $D$ ,  $\epsilon$  from (31) may be substituted directly into (20) to determine  $E_p$ . One may then add  $E_p$  to the bounds on  $E_s$  and use (15) to bound the temperature due the combined effect of shock and plastic work heating.

In the aforementioned, azimuthal symmetry is assumed. It is worth noting, however, that expansion beyond a critical point is unstable, and after a period of subsequent instability growth, the liner will fail. A band of ductile material being stretched will undergo plastic instability when the relative increase in the yield strength  $dY/Y$  due to work hardening over a time interval  $dt$  falls below the relative decrease in the band’s cross-sectional area  $dA/A$ . In the incompressible limit, this occurs when [30]  $Y = dY/d\epsilon$ . From (17), neglecting thermal softening, this condition is met when  $\epsilon$  reaches the following value, which corresponds to the given radius, based on (31)

$$\epsilon_p = \begin{cases} n - \frac{1}{\beta} - \epsilon_i, & \text{if } n - \frac{1}{\beta} - \epsilon_i < \epsilon_c \\ \epsilon_c, & \text{if } n - \frac{1}{\beta} - \epsilon_i \geq \epsilon_c \end{cases}$$

$$R_p = R_0 \exp \left[ \frac{\sqrt{3}}{2} \epsilon_p - \frac{V_r}{2D} \right]. \quad (33)$$

If this expression yields  $R_p < R_0$ , then expansion is unstable from the onset and  $R_p = R_0$  may be used instead.

### D. Tabulated Results for a Few Metals

Table I tabulates shock and plastic work heating estimates for a few metals for the case of a cylinder driven by LX-14 to radial speed  $V_r = 2702$  m/s.  $D = 8800$  m/s,  $\rho_x = 1835$  kg/m<sup>3</sup>, and  $\gamma_j = 2.947$  are used for LX-14 [2], based on parameter set 360 A of the cited reference.  $E_x$  is taken to be 95% that of HMX [22] (LX-14 is HMX with 5% binder), giving  $\sqrt{2E_x} = 2895$  m/s.  $P_1$  is calculated by the method described in Section V-B. The assumed  $V_r$  corresponds to an Al6061-T6 cylinder with inner radius 3.175 cm and wall thickness 0.635 cm, based on (32). It is presumed that we adjust the wall thickness to give the same  $M$  and, therefore  $V_r$ , for the other metals tabulated.

Given  $V_r/D = 0.307$ ,  $P_1$  for the different metals, and the Steinberg parameters for the solid, the heating terms may be found.  $E_1$  is calculated from (11). Bounds on  $E_s$  are calculated from (14).  $E_p$  is calculated from (20) at radius  $R = 2R_0$  [ $\epsilon = 0.978$  from (31)] for the cases where  $E_s$  equals the lower and upper bounds due to shock heating (max and min here refer to  $E_s$ ). The respective temperatures at each bound and stage are found from (13) for  $E_1$  and from (15) for the other (zero pressure) terms. The expansion factor for onset of instability  $R_p/R_0$  is found from (33).  $S_2 = S_3 = \epsilon_i = 0$  for the tabulated alloys. Silver is included since its high  $R_p/R_0$  and unsurpassed electrical conductivity make it an intriguing, albeit expensive, option for an explosive generator armature.

## VI. COMPARISON WITH CALE 2-D SIMULATIONS

Results of a two-dimensional (2-D) shock hydro simulations by program CALE [8], [9] are presented for comparison with the Al 6061-T6 and Cu analytic approximations, and to better quantify  $E_s$  for which we have, at present, only broad bounds. We use 30-cm-long liners with the same inner radius and mass as before and loaded with LX-14, for these simulations. The LX-14

TABLE I  
MATERIALS PROPERTIES AND PREDICTED SPECIFIC ENERGIES AND TEMPERATURES FOR VARIOUS METALS

	Al 6061-T6	Al 1100-0	Cu OFHC	SS 304	W	Ag
$C_0$ (m/s)	5240	5390	3940	4570	4030	3270
$S_1$	1.40	1.339	1.489	1.49	1.237	1.55
$\gamma_0$	1.97	1.97	2.02	1.93	1.67	2.4
$b$	0.48	0.48	0.47	0.50	0.38	0.56
$Y_0$ (MPa)	290	40	120	340	2200	50
$Y_{\max}$ (MPa)	680	480	640	2500	4000	660
$\beta$	125	400	36	43	24	28
$n$	0.10	0.27	0.45	0.35	0.19	0.8
$B/10^{-4}$ (K $^{-1}$ )	6.16	6.16	3.77	4.55	1.38	4.36
$\rho_0$ (kg/m $^3$ )	2703	2707	8930	7900	19,300	10,490
$C$ (J/kgK)	885	884	383	423	129	233
$P_1$ (GPa)	19.6	19.8	23.7	24.0	27.3	23.5
$E_1, E_s$ max (kJ/kg)	578	575	155	158	51.0	148
$E_s$ min (kJ/kg)	108	103	21.8	19.3	3.46	25.9
$E_p$ min (kJ/kg)	136	52.1	44.6	109	159	82.1
$E_p$ max (kJ/kg)	88	33.6	38.6	923	151	62.3
$T_1$ (K)	536	528	437	413	366	525
$T_s$ min (K)	417	411	355	344	327	406
$T_s$ max (K)	901	901	684	659	691	887
$T_p$ min (K)	561	467	466	593	1535	549
$T_p$ max (K)	987	935	777	864	1829	987
$R_p/R_0$	1	1.08	1.24	1.24	1	1.66

is detonated at the left end of the cylinder on the  $z$ -axis ( $r = z = 0$ ) at time  $t = 0$ . The simulations also assume the Steinberg model for the metal, so the test here is of the accuracy of our analytic approximations to the Steinberg model, as opposed to the model itself. Instead of the C–J EOS for the LX-14 products, though, CALE uses the Jones–Wilkins–Lee (JWL) EOS [31] with coefficients [2]  $A = 11.65$ ,  $B = 0.5572$ ,  $R_1 = 5.4$ ,  $R_2 = 2.0$ , and  $\omega = 0.45$ . These parameters are taken from same consistent set of data (360 A) as the C–J parameters used for the analytic model for maximum consistency. Note, though, that several alternative choices for LX-14 JWL coefficients are available in this reference and others [32], [33].

Fig. 1 is a pressure map closeup of the Al 6061-T6 run  $30 \mu\text{s}$  after detonation, when the detonation wave has reached  $z \approx 26.4$  cm. One can see here the prompt detonation products (contour 9), the high pressure region behind the initial Al shock wave (contours 5 and 6), and the much lower pressure of the second shock transmitted outward through the Al (contour 1). Details are blurred due to the initial square mesh length of 0.714 mm. The peak pressure behind the Al shock is  $P_1 \approx 20$  GPa, very similar to the value obtained by Neil’s method.

Fig. 2 shows the time history of total internal energy density of a fluid element in the Al 6061-T6 CALE simulation midway

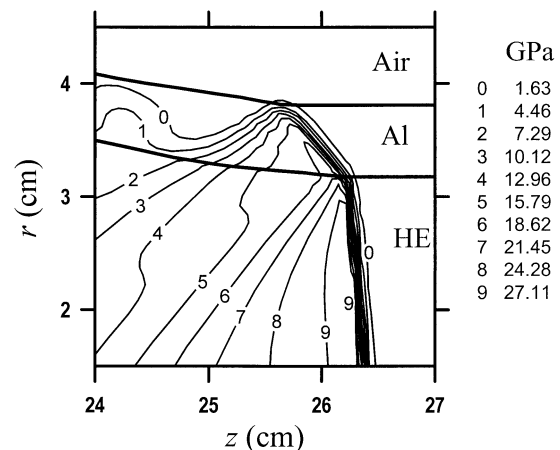


Fig. 1. Pressure map at  $30 \mu\text{s}$  of a CALE simulation of a 3.81 cm OD, 0.635 cm thick, 30 cm long Al 6061 T-6 tube filled with LX-14 and detonated on axis at the left end.

between the ID and the OD of the Al (to minimize edge effects due to the finite mesh size) and initially at  $z = 16$  cm (solid line). The element’s radius increases by a factor of two at  $t = 34.4 \mu\text{s}$ , as labeled by the cross hairs on this curve. The results of the analytic model’s upper and the lower bounds on

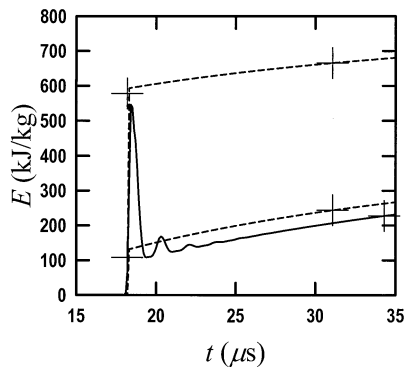


Fig. 2. Internal energy density versus time for Al 6061-T6 loaded with LX-14 midway between ID and OD of the cylinder, initially at  $z = 16$  cm. CALE simulation (solid line). Upper and lower bounds from analytic model (dashed line). Cross hairs signify upper and lower bounds on (left) dissipated shock heating and (right) the time on the respective curves where the radius has doubled.

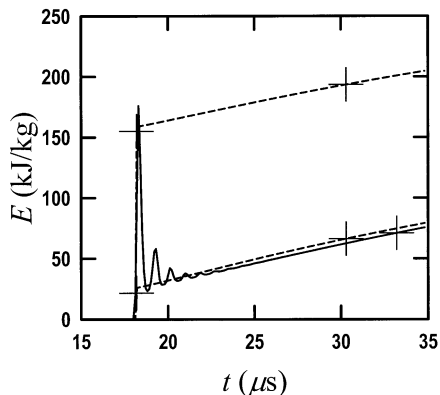


Fig. 3. Same plot as Fig. 2, but for Cu (1/2 hard) loaded with LX-14.

$E_s + E_p$  are overlaid. Here, we assume  $E_s$  is instantaneously thermalizes upon shock transit and that thereafter the liner expands at the Gurney speed [(32)]  $V_r = 2702$  m/s in accord with (30), with only plastic heating occurring during expansion. The initial radius used for calculating plastic strain is that at mid wall. The difference between shock heating, as signified by the cross hairs at  $E_s$  min and  $E_s$  max, and the start of the energy ramp up is the initial plastic work due to shear as the metal is assumed to jump suddenly to speed  $V_r$ . As with  $P_1$ , there is good agreement between the two models in regard to  $E_1$  behind the initial Al shock (recall this equals  $E_s$  max, labeled by the upper left cross hairs). There is also reasonable agreement between the two models after shock dissipation ( $t \approx 23 \mu\text{s}$ ) provided we assume  $E_f \approx E_f$  min. The reason for this is clear from the small magnitude of the second shock ( $t \approx 20 \mu\text{s}$ ). Apparently, the Al rarefaction wave efficiently couples to the explosive products, reflecting very little energy back outward as a second shock.  $E_s \approx E_s$  min, then, may be assumed for HE driving Al. As the liner expands, though, the analytic model overestimates  $E_p$  versus time. The reason for this is that plastic strain, and therefore heating, is primarily a function of expansion factor [(31)], and the Gurney equation overestimates the average speed of the liner during the period shown. The expansion velocity at the doubled radius of the Al in the CALE run is only  $V_r = 2500$  m/s,

with 90% of this not attained until  $t = 23 \mu\text{s}$  ( $5 \mu\text{s}$  after shock arrival). The energy discrepancy is significantly less (analytic is 6% higher) if one compares the models at the point where the radius at mid wall has doubled (right cross hairs).

Fig. 3 shows the same plot as Fig. 2, but for the Cu cylinder. Here, the analytic model's lower bound results in an energy density at doubled radius 5% lower than for the CALE run. The analytic value there being lower this time may be due to the (much denser) Cu having a greater impedance mismatch to LX-14 than Al, resulting in the second shock having a greater relative contribution. The Gurney speed overestimates  $V_r$  by about the same amount as it did for the Al run.

#### ACKNOWLEDGMENT

The authors wish to thank J. B. Chase for valuable assistance with the installation and operation of program CALE.

#### REFERENCES

- [1] M. Lehr, G. Baca, D. Chama, K. Hackett, T. Hussey, J. Kiuttu, D. Shiffler, J. Graham, W. Sommars, D. Coffey, and T. Englert, "Explosive pulsed power experiments at the Phillips Laboratory," in *Dig. Tech. Papers, 11th IEEE Int. Pulsed Power Conf.*, G. Cooperstein and I. Vitkovitsky, Eds., 1997, pp. 579–584.
- [2] E. L. Lee, D. Breithaupt, C. McMillan, N. L. Parker, J. W. Kury, C. M. Tarver, W. Quirk, and J. Walton, "The motion of thin metal walls and the equation of state of detonation products," in *Proc. 8th Symp. (Int.) Detonation, Albuquerque, NM*. Silver Spring, MD: Naval Surface Weapons Center, 1985, Report NSWC MP 86-194 (preprint available as LLNL Report UCRL-91490, Rev. 1), p. 613.
- [3] J. B. Chase, D. Chato, G. Peterson, and P. Pincosy, "CAGEN: A modern, PC based computer modeling tool for explosive MCG generators and attached loads," in *Dig. Tech. Papers, 11th IEEE Int. Pulsed Power Conf.*, G. Cooperstein and I. Vitkovitsky, Eds., 1997, pp. 1005–1009.
- [4] D. J. Steinberg, "Equation of state and strength properties of selected materials (revised)," Lawrence Livermore Nat. Lab., Tech. Rep. UCRL-MA-106439, change 1, Feb. 1996.
- [5] L. Knopoff, "Solids: Equations of state of solids at moderately high pressures," in *High Pressure Physics and Chemistry*, R. S. Bradley, Ed. New York: Academic, 1963, pp. 227–245.
- [6] D. J. Steinberg, S. G. Cochran, and M. W. Guinan, "A constitutive model for metals applicable at high-strain rate," *J. Appl. Phys.*, vol. 51, pp. 1498–1504, 1980.
- [7] D. J. Steinberg and C. M. Lund, "A constitutive model for strain rates from  $10^{-4}$  to  $10^6$  s $^{-1}$ ," *J. Appl. Phys.*, vol. 65, pp. 1528–1533, 1989.
- [8] R. E. Tipton, "A 2D Lagrange MHD code," in *Megagauss Technology and Pulsed Power Applications*, C. M. Fowler, R. S. Caird, and D. J. Erickson, Eds. New York: Plenum, 1987, 4th Int. Conf. Megagauss Magnetic Field Generation and Related Topics, also available as LLNL Report UCRL-94277, p. 299.
- [9] —, *CALE Users Manual*. Livermore, CA: Lawrence Livermore Nat. Lab., 1991, MS L-35.
- [10] D. J. Cagliotro, D. A. Mandell, L. A. Schwalbe, T. F. Adams, and E. J. Chapyak, "MESA 3D calculations of armor penetration by projectiles with combined obliquity and yaw," *J. Impact Eng.*, vol. 10, 1990.
- [11] W. H. Lee, "Two-dimensional Lagrangian method for elastic-plastic flow," *Comput. Methods Appl. Mech. Eng.*, vol. 156, pp. 149–169, 1998.
- [12] D. J. Steinberg, "Constitutive models used in computer simulation of time-resolved shock-wave data," Lawrence Livermore Nat. Lab., Tech. Rep. UCRL-93703, Rev. 1, Apr. 1987.
- [13] R. E. Peterkin, Jr. and M. H. Frese, "A material strength capability for MACH2," Mission Research Corp., 1720 Randolph Rd., SE, Albuquerque, NM, Tech. Rep. MRC/ABQ-R-1191, Nov. 1989.
- [14] J. M. Walsh, M. H. Rice, R. G. McQueen, and F. L. Yarger, "Shock-wave compressions of twenty-seven metals. equations of state of metals," *Phys. Rev.*, vol. 108, pp. 196–216, 1957.
- [15] W. E. Boyce and R. C. DiPrima, *Elementary Differential Equations*, third ed. New York: Wiley, 1997.

- [16] Y. B. Zel'dovich and Y. P. Raizer, *Physics of Shock Waves and High-Temperature Hydrodynamic Phenomena*. New York: American Elsevier, 1966.
- [17] H. Knoepfel, *Pulsed High Magnetic Fields*. New York: American Elsevier, 1970.
- [18] A. S. Kahn and S. Huang, *Continuum Theory of Plasticity*. New York: Wiley, 1995.
- [19] R. W. Gurney, "The initial velocities of fragments from bombs, shells, and grenades," Brooks Research Laboratory, Tech. Rep. 405, 1943.
- [20] N. E. Hoskin, W. S. Allan, W. A. Bailey, J. W. Lethaby, and I. C. Skidmore, "Motion of plates and cylinders driven by detonation waves at tangential incidence," in *Proc. 4th Symp. (Int.) on Detonation*. Washington, DC: Office of Naval Res., 1965, report ACR-126, pp. 14–26.
- [21] O. E. Jones, "Metal response under explosive loading," in *Behavior and Utilization of Explosives in Engineering Design 12th Annual Symp.*, L. Davison, J. E. Kennedy, and F. Coffey, Eds. Albuquerque, NM: ASME (NM Section), 1972.
- [22] J. E. Kennedy, "Explosive output for driving metal," in *Behavior and Utilization of Explosives in Engineering Design 12th Annual Symp.*, L. Davison, J. E. Kennedy, and F. Coffey, Eds. Albuquerque, NM: ASME (NM Section), 1972, pp. 109–124.
- [23] E. L. Lee and H. Pfeifer, "Velocities of fragments from exploding metal cylinders," Lawrence Livermore Nat. Lab., Tech. Rep. UCRL-50545, Jan. 6, 1969.
- [24] J. W. Kury, H. C. Hornig, E. L. Lee, J. L. McDonnel, D. L. Ornellas, M. Finger, F. M. Strange, and M. L. Wilkens, "Metal acceleration by chemical explosives," in *Proc. 4th Symp. (Int.) on Detonation*. Washington, DC: Office of Naval Res., 1965, Rep. ACR-126, pp. 3–13.
- [25] T. Neal, "Perpendicular explosive drive and oblique shocks," in *Proc. Sixth Symposium (International) on Detonation*. Arlington, VA: Office of Naval Res., 1976, Rep. ACR-221, pp. 602–611.
- [26] A. H. Shapiro, *The Dynamics and Thermodynamics of Compressible Fluid Flow, Vol. I*. New York: Wiley, 1953.
- [27] W. Fickett and W. C. Davis, *Detonation*. Los Angeles, CA: Univ. of CA Press, 1979.
- [28] Y. B. Zel'dovich and A. S. Kompaneets, *Theory of Detonation*. New York: Academic, 1960.
- [29] G. E. Duvall and G. R. Fowles, "Shock waves," in *High Pressure Physics and Chemistry*, R. S. Bradley, Ed. New York: Academic, 1963, vol. 2, pp. 209–291.
- [30] J. Chakrabarty, *Theory of Plasticity*. New York: McGraw-Hill, 1987.
- [31] E. L. Lee, H. C. Hornig, and J. W. Kury, "Adiabatic expansion of high explosive detonation products," Lawrence Livermore Nat. Lab., Tech. Rep. UCRL-50411, May 2, 1968.

- [32] H. Hornberg, "Determination of fume state parameters from expansion measurements of metal tubes," *Propellants, Explosives, Pyrotechnics*, vol. 11, pp. 23–31, 1986.
- [33] R. E. Tipton, "Eos coefficients for the CALE code for some materials," CALE documentation, unpublished.



**Edward L. Ruden** (M'96) received the Ph.D. degree in physics studying plasmas from the University of California, Irvine, in 1988.

Since then, he has performed research in the area of high-energy density states of matter for the Air Force Research Laboratory's Directed Energy Directorate, Kirtland AFB, NM, and its organizational predecessors. He has developed several interferometric systems for the diagnosis of plasmas using coherent radiation sources across a broad spectrum: millimeter wave, far IR, visible, and UV. In addition, he has extensive experience in experimental, analytic, and computational efforts involving continuum dynamics of all phases of matter.



**Gerald F. Kiuttu** (M'83) received the B.S. degree in engineering science from Arizona State University in 1975, and the M.S. and Ph.D. degrees in nuclear engineering (plasma physics) in 1980 and 1986, respectively. His dissertation involved development of time- and space-resolved soft X-ray spectroscopic techniques.

He served in the Air Force and was stationed at the Air Force Weapons Laboratory from 1975 to 1980, where he worked on optical and X-ray spectroscopic diagnostics for high-energy plasmas. In 1982, he joined the staff of the Plasma Physics Division, Mission Research Corporation, Albuquerque, NM. As a senior scientist there, he worked in the areas of pulsed power, intense electron beam physics, plasma diagnostics, plasma ion sources, and high power microwaves. In 1991, he returned to the Air Force Phillips Laboratory's High Energy Plasma Division, where he worked on plasma diagnostics and led the compact toroid research program until 1996. He is currently Pulsed Power Technology Team Leader in the Directed Energy Directorate of the Air Force Research Laboratory, Kirtland AFB, NM, where he directs pulsed power, and related research.